2024 IEEE International Conference on Robotics and Automation (ICRA 2024)
May 13-17, 2024. Yokohama, Japan

Lightweight Untethered Soft Robotic Fish

Xiangxing Wang[1], Xuan Pei[1], Xinyang Wang[2], Taogang Hou[1,*]

***Abstract*—Aquatic organisms, due to soft body structure and high agility, have inspired many biomimetic robots. However, considering the issues of insulation and waterproofing, as well as the driving module of soft materials, their control systems are usually larger and heavier. Therefore, small underwater robots often tethered, i.e., it cannot integrate energy and control systems onto the body, which greatly limited in its working range and activity mode. This paper presents a small untethered bionic manta ray. The robotic fish is driven by dielectric elastomer actuators (DEA), which controls the double wing structure on both sides by the central muscle part to simulate the process of the manta ray's lateral fins fanning to propel itself forward. And the flexible printed circuit board (FPC) constitutes the body of the fish and is also an independent energy control system. The electronic components are evenly distributed on the double-wing structure of the robotic fish to realize the integration of the energy control system. This circuit system can be powered by a small lithium battery and output a periodic voltage to drive the motion of the robotic fish. The masses of our tethered and untethered fish are 1.9g and 5.1g respectively. The swimming speed of these two types of fish can reach 42.5mm/s and 17.0 mm/s. And this design principle can be extended to the research and design of various flexible devices and soft robots.**

I. Introduction

Manta rays are special marine creatures with a pair of wings. During the swimming process, the pectoral fins swing up and down by muscles, pushing the water around the pectoral fins and pushing the body forward through the reaction force. Its soft wings provide excellent paddling ability, and its wide biplane structure allows manta rays to effectively utilize the energy of liquids and achieve more efficient gliding movements. In addition, the strong driving force of the pectoral fin muscles enables the wings to complete periodic swings in a short period of time, ensuring the speed and agility [1]. The bionic design of this structure can improve the performance of robots.

The application of traditional rigid robots in specific scenarios is limited due to their fragile structure and large volume [2]. The soft robots have made up for these shortcomings of rigid robots [3]. By imitating the soft body structure of natural organisms, soft robots can be inspired to design biomimetic robots with richer functions and better performance [4]. Due to its ability to adapt to various unstructured environments and its ability to drive actions more freely and flexibly, it has become a hot topic. At present, typical software driven materials include shape memory alloys (SMA) [5], ionic polymer metal composites (IPMC) [6], dielectric elastomers (DE) [3,7,8,9], responsive hydrogels [10], aerodynamic structures, chemical reaction expanded fluid networks and living cells. Among them, DE has the characteristics of softness, high energy density, high power-to-weight ratio, fast response speed [11], silence, energy saving, etc., its power consumption is on the order of mW [25], and has broad application prospects [12,13]. On the other hand, DE is driven by electrical voltage, so it can better integrate with electronic control systems [14,24], facilitating the integrated processing of energy systems. Based on the above advantages, DE is a good choice for the driving material used for biomimetic robotic fish [15].

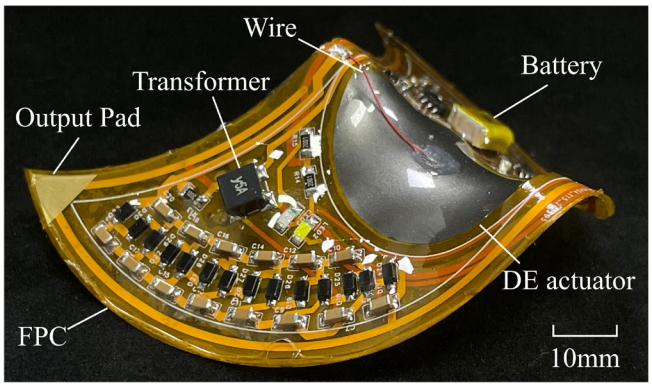

Figure 1. Soft machine manta ray driven by DEA and controlled by FPC.

Currently, extensive research has been conducted on DE driven underwater robots. However, due to the high voltage demand of DE for driving signals, its control system typically requires larger transformers and batteries to form. In addition, DE requires additional insulation and waterproof treatment operations when working underwater, which increases structural complexity. Therefore, most current DE-driven robotic fish cannot swim independently, but are powered by external drive control systems through wires [16]. The integrated untethered robotic fish are usually larger in size and heavier in weight [17], which seriously affects the movement performance and causes its swimming speed to drop significantly.

In this study, we propose a small, lightweight, and completely independent biomimetic soft robot fish (Fig.1), which is based on a dielectric elastomer actuator (DEA) and combined with a flexible printed circuit board (FPC) and surface mounted devices (SMD) electronic components to achieve the integration of energy control systems. The shape of robotic fish is similar to that of manta rays, with

Research was supported by the National Science Foundation of China (Grant No. 62103035); the Beijing Natural Science Foundation (Grant No. 3222016); the Young Elite Scientists Sponsorship Program by CAST (Grant No. 2022QNRC001); the Beijing Natural Science Foundation (Grant No. L231004) and China Postdoctoral Science Foundation (Grant No. 2021M690337).

[1] Xiangxing Wang is with School of Automation and Intelligence, Beijing Jiaotong University.

[2] Xinyang Wang is with Department of Bioengineering, Imperial College London.

Correspondence: houtaogang@bjtu.edu.cn

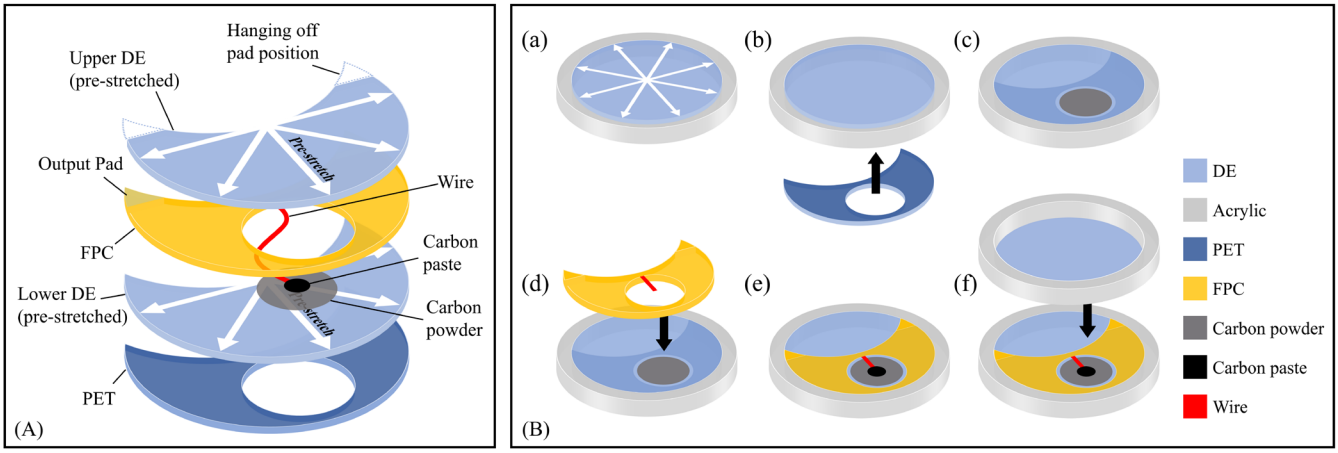

Figure 2. (A) Multi-layer structure of robotic fish. (B) Production process: (a) Pre stretching the DE film on an acrylic ring. (b) Paste butterfly shaped PET onto the lower surface of DE. (c) Apply carbon powder as a flexible electrode at the center hole position of PET. (d) Paste the FPC with a wire on the positive pole of the output end onto the upper surface of the DE. (e) Place the end of the wire at the center of the flexible electrode and apply carbon paste. (f) Cover the FPC with another pre stretched DE on the acrylic ring.

polyethylene glycol terephthalate (PET) as the support frame. DEA plays a muscular role by using surrounding water as electrodes [15,17], which can work normally in water and drive the swimming movements of manta rays. In addition, a corresponding energy and control system was designed and printed on a specially designed flexible PCB (printed circuit board) circuit. Select small and lightweight SMD components and distribute them on the PCB. This circuit is powered by a small 3.7V lithium battery and can generate high-voltage square wave electrical signals to drive DEA operation. The positive and negative poles of PCB output are connected to DEA and environmental water through wires and pads, respectively. A special design has been made to the structure of the robotic mermaid, achieving insulation and waterproofing measures for underwater DEA and PCB circuits, and achieving independent driving of the untethered robotic fish.

II. Design

A. Skeleton

We have designed a special double wing structure for robotic fish, which simulates its swimming process by driving its wings to vibrate like a manta ray (Fig.2). PET material, due to its moderate hardness and strong toughness, has good physical and mechanical properties, and is commonly used as a flexible support frame in soft robot structures [19]. In this study, a PET thin plate with a pair of side fin shapes is used as a biomimetic fish flexible frame to simulate the biplane structure of manta rays. Cut a 0.4mm thick PET board into a butterfly shape, with the wings of the robotic fish extending backwards on both sides. Reserve a hole in the center of PET as the location for placing the driving material, exerting the muscle's function. During swimming, muscles are controlled by control signals to periodically expand and contract, driving the lateral fins on both sides to swing up and down, achieving the vibration of mechanical fish wings similar to manta rays.

B. Actuator

In order for DEA to function as a muscle, the actuator needs to be pre stretched axially and placed in the center hole of the machine wing structure. Based on the principle of origami [14], PET serves as a supporting framework, changing its shape as DEA expands and contracts, resulting in three-dimensional stretching and folding changes. When no voltage is applied, DEA contracts, and PET compresses towards the center under the action of force, forming a folded state similar to a saddle shaped surface shape [20]. Due to the small width and elasticity of the butterfly shaped PET holes at the upper and lower ends, the folding amplitude of these two points is relatively large when the saddle surface is folded. The overall shape is manifested as the wing structure of a robotic fish folding along the centerline, similar to the process of a manta ray swinging its side fins inward. When voltage is applied to DEA, DEA extends and PET returns to a flat shape due to its own elasticity. At this point, the biplane structure returns to an outward extension state, which is the movement of the manta ray to unfold its lateral fins. By controlling the periodic swing of the wings using DEA, the surrounding water is drawn backward, pushing the robotic fish forward.

C. Drive control system

We designed a circuit as a drive control system that can generate a specific high-voltage square wave electrical signal to drive DE to achieve periodic action. The main circuit structure is shown in Fig.4. Select small SMD electronic components to meet the overall integration requirements of the robotic fish and distribute and solder them onto printed circuit boards. Use a FPC designed to have the same shape as PET as the board to adapt to the overall shape of the robotic fish. FPC is a highly reliable and flexible printed circuit board with the characteristics of high wiring density, light weight, thin thickness, and free bending and folding [18,21,22]. It can better meet the integration requirements of the energy control system for robotic fish. By pasting FPC onto PET, the soft and thin FPC can not only function as a wire, but also serve as a flexible frame for the robotic fish, supporting and guiding deformation together with PET.

III. METHODS

A. Structure

The overall structure of the robotic fish is as shown in the Fig.2(A). It uses the surrounding water as an electrode to achieve insulation and waterproof treatment to ensure the normal use of DEA in the water. The soft robotic fish is composed of two layers of dielectric elastomer (DE), a PET film cut into a butterfly shape (with a hole in the middle), and a flexible PCB. The DEA that drives the robotic fish to complete its movement is composed of DE and PET, with the former serving as an active deformation layer and the latter serving as a flexible support frame. Sandwich the FPC between two pieces of DE and glue it to the PET. The positive output of the FPC is connected to the flexible electrode in the middle of the DE through a thin wire, and the negative output is connected to the surrounding water through the tail pad. The lower layer of DE not only functions as a muscle driver, but also serves as a glue connection between PET and FPC. The upper DE serves as a waterproof layer and can provide waterproof functions for PCB and flexible electrodes. The detailed manufacturing process is shown in Fig.2(B).

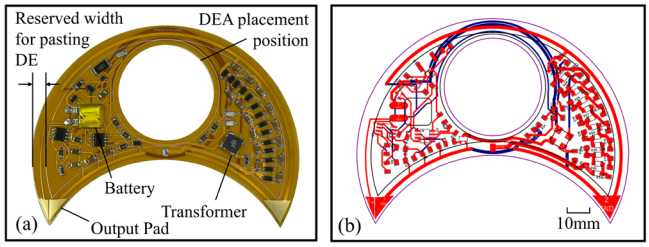

Figure 3. (a) Front view of drive control system circuit FPC. (b) PCB design diagram.

To meet the requirements of integration and miniaturization, SMD electronic components were selected to minimize the mass and volume of the robotic fish. Use freely bendable flexible PCB as a carrier for electrical interconnection of electronic components. During the component distribution design process, the impact on the motion performance of the robotic fish needs to be considered. The components of the circuit are designed to be centered as close to the centerline as possible to reduce the torque on the wing and reduce the effect of component weight on the amplitude and frequency of wing oscillations. This also allows a certain distance between the distribution area of electronic components and the outer edge of the PCB, leaving a certain width for the DE film to be pasted. The design also takes into account the symmetrical weight of the components distributed on both sides of the wings to prevent the robotic fish from being unable to swim in a straight line due to uneven weight distribution on both sides. The physical diagram and PCB design diagram of the circuit are shown in the Fig.3.

B. Circuit

1) Boost

The deformation of DE requires a voltage of up to 3.5kv to drive, and excessive voltage will cause electrical breakdown damage to DE. Based on this characteristic, a small boost circuit is designed. This circuit is powered by a 3.7V lithium battery and outputs a square wave signal with an amplitude of approximately 4kV and adjustable frequency. As one of the largest components in the entire circuit [18], the selection of the transformer determines the overall size of the circuit. This study selected TTRN-0635H-000-T Y5A SMD flash transformer with a turn ratio of 1:26. The transformer has a small size, flat appearance, and low height, and will not damage the overall structure of the robotic fish after welding in the circuit. The transformer is driven by an SS8050 transistor. The high-frequency driving square wave is input to the base of the triode through the current limiting resistor to control the on-off of the triode. The amplification effect of the transistor is used to generate a large sudden change current in the primary winding circuit of the transformer. Due to the non-mutating characteristics of the inductor current, a higher AC voltage can be generated at the input end of the transformer. Through the principle that the transformer voltage ratio is equal to the turn ratio, the voltage is boosted to about 300V AC. Connect the transformer output to the voltage multiplier rectifier circuit. Using the principle that the capacitor voltage does not change suddenly, the AC input voltage is greatly increased and rectified into a high voltage, small current DC output. The robotic fish circuit uses a 14 times voltage multiplier rectifier circuit to convert a 300V AC input into a 4kV DC output. Through this method, 4kv high voltage can be generated using only a small transformer and battery, greatly reducing the size and quality of the circuit. The high voltage generated by this method has a small power output and limited accuracy, but it precisely meets the characteristics of DE's low demand for driving signal current and accuracy.

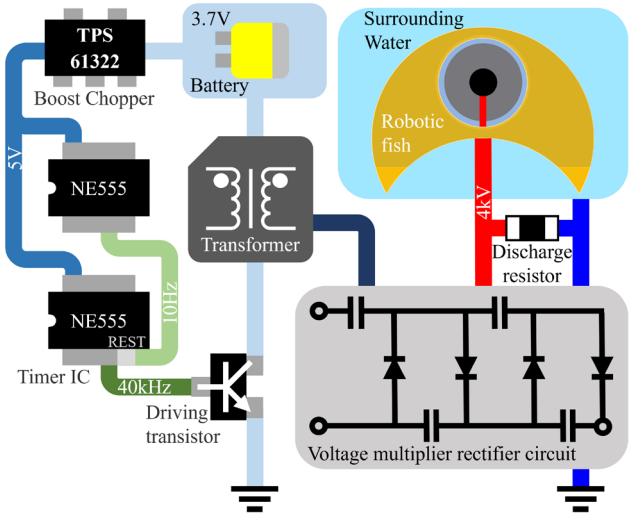

Figure 4. Schematic diagram of the overall circuit structure and connection method with DE.

2) Frequency

This circuit uses two NE555 chips to output square wave signals of different frequencies. One of the outputs is a square wave signal with adjustable frequency, which is used to control the oscillation of the wing. The other is a square wave that drives the transformer to boost the voltage, with a frequency of about 40khz and a duty cycle of 60%. Connect the output signal of the first chip to the reset pin of the second chip and connect the output of the second chip to the base of the transistor. The second chip is turned on or off through the

high-low level conversion of the square wave output of the first chip, and controls whether the transformer is driven. In this way, the generation and cutoff of high-voltage voltage are controlled and converted into a frequency-controllable high-voltage square wave signal to drive DE period scaling.

3) Discharge Resistor

The deformation of DE is caused by the interaction of charge forces between the charges distributed at the two poles, which is similar to the charging and discharging process of capacitors. Therefore, the stretching process of DE can be analogized to the charging and discharging process of capacitors. During the contraction process of DE, the charges distributed at both ends of DE are consumed in some way, similar to the process of releasing voltage from a fully charged capacitor.

According to the voltage over time formula of capacitors:

$$V_t = V_0 + (V_1 - V_0) \times (1 - e^{-\frac{t}{RC}}) \tag{1}$$

And the formula for capacitor charging and discharging time:

$$t = RC \times \ln(\frac{V_1 - V_0}{V_1 - V_t}) \tag{2}$$

Where C is the capacitance value, fixed and unchanged. R is the resistance value. The discharge speed of a capacitor is related to the resistance value of its parallel resistor. The larger the resistance, the slower the discharge, while the smaller the resistance, the faster the discharge.

Similarly, the contraction speed of DE is related to the resistance value of its parallel resistor. When DE does not have a parallel resistor, its two ends are open. When the voltage applied to both ends of DE is withdrawn, the surface distributed charge slowly dissipates through its own resistance. A resistor can be connected in parallel at both ends of DE as a discharge resistor [15]. When the voltage is withdrawn, the charges at both ends of DE can be consumed through this resistor. This can significantly improve the contraction speed of DE and the response speed of DEA.

The parallel resistance connected in DE will have a partial voltage effect. When applying driving voltage to DE, due to the presence of parallel resistors, a 4kV driving voltage cannot be fully applied to both ends of DE. The decrease in driving voltage will affect the expansion amplitude of DE. Therefore, adding a voltage reducing resistor also has certain drawbacks. The selection of the voltage discharge resistor value should be considered from many aspects.

IV. Experiments and Discussion

The output power of the robotic fish is provided by the battery of the load. The circuit system converts electrical energy into kinetic energy for the robotic fish to move forward. To test the output power of the robotic fish, we designed multiple sets of experiments to test its performance under wired power and the effects of different parameters. The tethered and untethered robotic fish use the same control system and structure The difference is that the energy and control system of the former is not integrated into the body. It is driven by an external system and connected through a thin wire with an outer diameter of 0.28mm. Compared with the cordless robotic fish, its structure is simpler, so its wings swing faster and to a greater extent. We focus on the process of body shape changes of the robotic fish under the influence of parameter changes. Using a wired robotic fish can more visually demonstrate this aspect of performance. Therefore, the experiments were all under the tethered circumstances.

A. Frequency and Amplitude

Under a certain resistance, the swimming speed of robotic fish is mainly affected by the amplitude and frequency of wing oscillation. We designed several sets of experiments to change several parameters that have a significant impact on the frequency and amplitude of robotic fish wing oscillations. The swing amplitude of the robotic fish wings is related to the driving voltage, and the larger the voltage, the greater the swing amplitude. The experiment generates different driving voltages by changing the input voltage of the driving control circuit [23]. We tested the effect of driving voltage within the range of around 3.8kV on the swimming speed of robotic fish. Excessive voltage may cause DE electrical breakdown, so the maximum test voltage is 4kV.The pectoral fin oscillation frequency of manta rays is generally 0.3 Hz, with a maximum oscillation frequency of 0.6 Hz. However, considering the differences in body size between robotic fish and real manta rays, we set the oscillation frequency of biomimetic fish to be between 1-20Hz. During the experiment, the oscillation frequency of the robotic fish wings was changed by controlling the frequency of the square wave signal input to the reset pin of the voltage driver chip. The variation of swimming distance of robotic fish over time. The untethered robotic fish has a downstream speed of 17.0mm/s at a fin flapping frequency of 10hz.

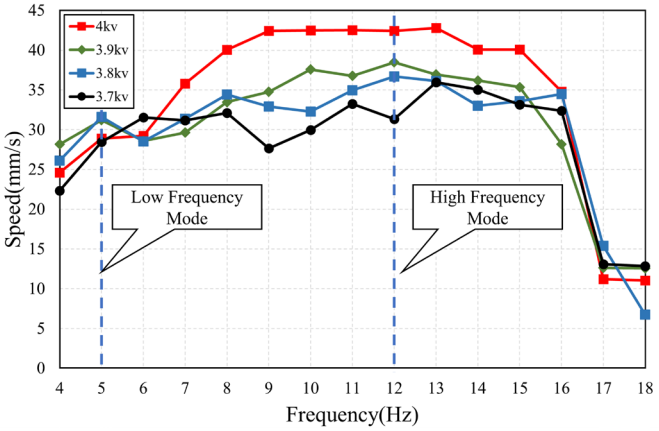

Figure 5. The speed versus frequency curve under driving voltages of 3.7, 3.8, 3.9 and 4 kilovolt under tethered circumstances.The higher the driving voltage, the faster the speed. The velocity curve with frequency shows a single peak distribution, reaching the fastest at around 13Hz at 42.7mm/s.

As shown in Fig.5, it can be concluded that within a certain range, as the voltage increases, the swing amplitude of the robotic fish wings increases, and its swimming speed also increases. In the range of 4hz~13hz, the higher the frequency, the faster the wing swinging speed and the faster the swimming speed. However, after the frequency exceeds 13Hz,

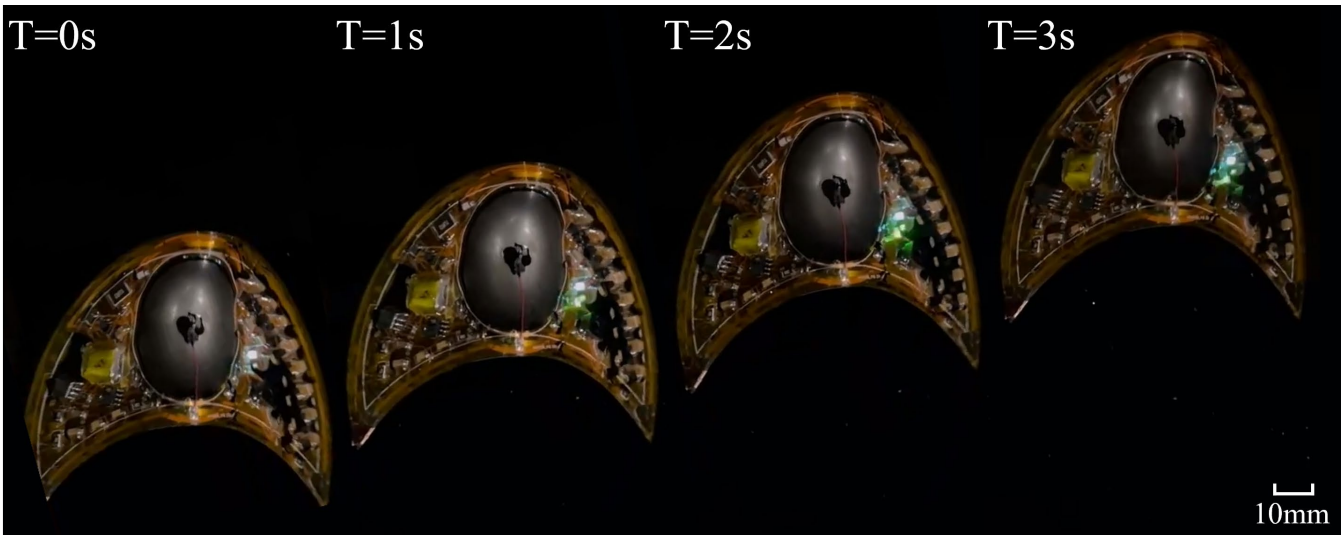

Figure 6. The variation of swimming distance of robotic fish over time. The untethered robotic fish has a downstream speed of 17.0mm/s at a fin flapping frequency of 10hz.

due to the limitation of material response speed, the robotic fish wings cannot fully extend within one cycle, resulting in a decrease in swing amplitude and a slower speed. Therefore, we define these two ranges as two differentiated modes, 4-8hz is the low-frequency mode, and 8-15hz is the high-frequency mode.

B. Duty Cycle

During a single flapping cycle, the wings are divided into a deployment process and a contraction process. The deployment of the wings is to accumulate energy, while contraction is the main process that provides thrust. If the deployment time is too short, it may cause the expansion amplitude of the wings to be too small, resulting in the contraction of the wings being unable to provide high thrust. If the contraction time is too short, it will reduce the application time of the thrust. An unreasonable duty cycle will reduce the power of a single propulsion.

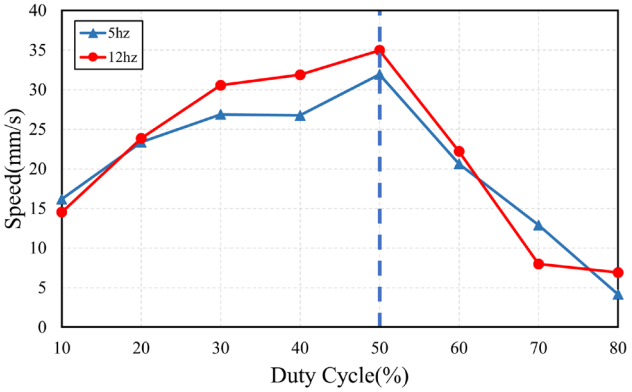

Figure 7. Curve of the variation of speed with the duty cycle of the control square wave signal at different frequencies. At a duty cycle of 50%, the deployment and contraction time reaches a balance, providing maximum propulsion power and achieving the fastest speed.

We designed an experiment to change the duty cycle of the control wing square wave to explore the impact of the deployment time and contraction time of the wings on the speed. Select 5Hz and 12Hz as low-frequency and high-frequency modes respectively and compare the impact of duty cycle on travel speed at different frequencies. Experimental results (Fig.7) show that when the duty cycle is 50%, the opening, closing and contraction of the robotic fish's wings reach a balance, and the swimming speed is the fastest.

C. Performance

1) Performance parameter

The mass, length, swimming speed and other data of the tethered and untethered fish in this study are shown in the TABLE 1. The energy and control system weighs only 3.2g, which makes the robot fish's body structure lighter, shorter and faster. At the same time, the structural combination with FPC greatly enhances the flexibility of the robotic fish's body. This is very helpful to improve the movement performance of the robotic fish.

TABLE I. COMPARISON OF BASIC PARAMETERS AND PERFORMANCE INDICATORS

Power Supply	The main parameters			
	Mass (g)	***Length (mm)***	***Absolute speed (mm/s)***	***Relative speed (body length /s)***
Tethered	1.9	75	42.5	0.57
untethered	5.1	75	17.0	0.23

2) Swimming process

Use a camera with a frame rate of 30 to record the swimming process of the robotic fish. The driving signal frequency is 5Hz and the voltage is 4kV. Record the position of the robotic fish in each frame (Fig.6) and calculate the instantaneous speed (Fig.8). Compare the instantaneous speed of the robotic fish within 1 second with the control signal. When the control signal is high level, the voltage applied to DEA is 4kv, and DE expands [17]. At this time, the robotic fish spreads its wings and can glide in the water at a speed of about 2mm/s relying on its own inertia. The structure of the

robotic fish's wide wings and its small size and low resistance greatly improve its energy utilization. When the control signal jumps to low level, DE shrinks rapidly. At this time, the robotic fish's wings quickly close together, using fluid energy to push itself forward. The light mass makes the acceleration very large, and the speed quickly increases to about 30mm/s. In summary, the lightweight and compact size of the robotic fish have greatly improved the movement performance of the robotic fish, allowing it to have higher energy utilization and faster swimming speed.

Compared with the tethered fish, the swimming speed of the integrated untethered robotic fish dropped to 50% of the original (42.5mm/s to 17.0mm/s). The increase in weight is the main reason for the decline in motion performance. The weight of the loaded system is 3.2g, accounting for 62.7% of the total mass of the untethered robotic fish (5.1g). Moreover, the increase in the weight of the wings caused by the components reduces the swing frequency and amplitude, reducing the thrust that can be provided. Under the condition of constant resistance, the heavier mass and smaller thrust cause the robotic fish to obtain lower acceleration, so the speed is significantly slowed down.

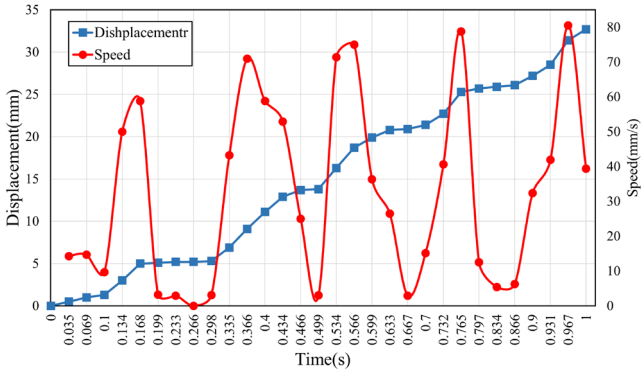

Figure 8. The curve of displacement and velocity over time at a frequency of 5Hz and a driving voltage of 4kV. The speed of robotic fish fluctuates periodically. At the moment of retracting the wings, the speed reaches its fastest.

V. Conclusion

To solve the problem that tethering of small bionic fish limits the range of activities, this study makes efforts from the aspects of structure and control. In terms of the structure of the fish, the FPC circuit board is directly used to design the shape of the fish, and SMD devices are used to reduce the weight of the fish, so that the untethered fish only adds 3.2g compared to the tethered type. In the control system mode, a small transformer controllable voltage boost method is designed to generate a high-voltage controllable frequency square wave. On the premise of meeting the driving conditions, the weight of the circuit is reduced and the response speed is increased. The optimal control frequency, duty cycle and driving voltage parameters were obtained through experiments. The swimming experiment verified that this tethered fish can swim underwater and achieved a swimming speed of 17.0mm/s. Compared with tethered fish, untethered fish are not restricted by wires and have a greater range of activities and flexibility. However, as the structural complexity increases, a certain degree of working stability and speed are lost. These performance improvements are the main research goals of untethered robots in the future. This type of configuration approach can potentially be applied to future research on the structural design and control methods of DEA robots.

There are still aspects of this study that need to be enhanced. Strengthen the structural design to increase swimming speed while ensuring working stability. Add a hydrodynamic design to the wings of the robotic fish to improve energy utilization. Design circuits to add more functions, such as underwater positioning, remote control, photography, etc., to put them into real application scenarios.

References

[1] Frank F, Christian S, Keith M, et al. Hydrodynamic Performance of Aquatic Flapping: Efficiency of Underwater Flight in the Manta[J]. Aerospace, 2016. DOI:10.3390/aerospace3030020.

[2] Zhakypov Z, Mori K, Hosoda K, et al. Designing minimal and scalable insect-inspired multi-locomotion millirobots[J]. Nature, 2019, 571(7765):381-386. DOI:10.1038/s41586-019-1388-8.

[3] Gao, D., Thangavel, G., Lee, J. et al. A supramolecular gel-elastomer system for soft iontronic adhesives. Nat Commun 14, 1990 (2023). https://doi.org/10.1038/s41467-023-37535-4

[4] T. Hou et al., "Design, Fabrication and Morphing Mechanism of Soft Fins and Arms of a Squid-like Aquatic-aerial Vehicle with Morphology Tradeoff," 2019 IEEE International Conference on Robotics and Biomimetics (ROBIO), Dali, China, 2019, pp. 1020-1026, doi: 10. 1109/ ROBIO49542. 2019. 8961447.

[5] Wang Z, Hang G, Li J, et al. A micro-robot fish with embedded SMA wire actuated flexible biomimetic fin[J].Sensors & Actuators A Physical, 2008, 144(2):354-360.DOI:10.1016/j.sna.2008.02.013.

[6] Su Y, Ye X, Guo S. An Autonomous Micro Robot Fish Based on IPMC Actuator[J]. Robot, 2010, 32(2):262-270. DOI:10.3724/SP.J.1218. 2010.00262.

[7] Carpi, Federico, Bauer, et al. Stretching Dielectric Elastomer Performance. [J]. Science, 2010. DOI: 10. 1126/ science. 1194173.

[8] Anderson IA, Gisby T A, Mckay T G, et al. Multi-functional dielectric elastomer artificial muscles for soft and smart machines[J]. Journal of Applied Physics, 2012, 112(4):041101-041101-20. DOI:10.1063/1. 4740023.

[9] Zhao X, Suo Z. Method to analyze programmable deformation of dielectric elastomer layers[J]. Applied Physics Letters, 2008, 93(25): 071101. DOI: 10. 1063/ 1. 3054159.

[10] Kim J, Hanna J A, Byun M, et al. Designing Responsive Buckled Surfaces by Halftone Gel Lithography[J]. Science, 2012, 335(6073): 1201. DOI: 10. 1126/ science. 1215309.

[11] Shintake, Jun, Cacucciolo, et al. Soft Biomimetic Fish Robot Made of Dielectric Elastomer Actuators[J]. Soft Robotics, 2018.

[12] Li T, Keplinger C, Baumgartner R, et al. Giant voltage-induced deformation in dielectric elastomers near the verge of snap-through instability[J]. Journal of the Mechanics & Physics of Solids, 2013, 61(2): 611-628. DOI: 10.1016/j.jmps.2012.09.006.

[13] Carpi F, Rossi DD, Kornbluh R, et al. Dielectric Elastomers as Electromechanical Transducers: Fundamentals, Materials, Devices, Models and Applications of an Emerging Electroactive Polymer Technology[J]. 2008.

[14] Yanhua Sun, Dengfeng Li, Mengge Wu, Yale Yang, Jingyou Su, Tszhung Wong, Kangming Xu, Ying Li, Lu Li, Xinge Yu, Junsheng Yu, Origami-inspired folding assembly of dielectric elastomers for programmable soft robots, Microsystems & Nanoengineering, Volume 8, Issue 1, 2022, Pages 37ISSN 2095-7106, https://doi.org/10.1038/ s41378-022-00363-5.

[15] Li, G., Chen, X., Zhou, F. et al. Self-powered soft robot in the Mariana Trench. Nature 591, 66–71 (2021). https://doi.org/10.1038/s41586-020-03153-z

[16] J. Shintake, H. Shea and D. Floreano, "Biomimetic underwater robots based on dielectric elastomer actuators," 2016 IEEE/RSJ International Conference on Intelligent Robots and Systems (IROS), Daejeon, Korea (South), 2016, pp. 4957-4962, doi: 10.1109/IROS.2016.7759728.

[17] Tiefeng Li. et al. Fast-moving soft electronic fish. Sci. Adv. 3, e1602045(2017). doi:10.1126/sciadv.1602045
[18] Z. Liu, "Reliability evaluation of FPC under bending stress," Proceedings of 2011 International Conference on Electronic & Mechanical Engineering and Information Technology, Harbin, China, 2011, pp. 2955-2958, doi: 10.1109/EMEIT.2011.6023667.
[19] L. Xu and G. Gu, "Bioinspired Venus flytrap: A dielectric elastomer actuated soft gripper," 2017 24th International Conference on Mechatronics and Machine Vision in Practice (M2VIP), Auckland, New Zealand, 2017, pp. 1-3, doi: 10.1109/M2VIP.2017.8211523.
[20] X. Wang, X. Pei, X. Wang and T. Hou, "Bionic Robot Manta Ray Based on Dielectric Elastomer Actuator," 2023 International Conference on Frontiers of Robotics and Software Engineering (FRSE), Changsha, China, 2023, pp. 387-392, doi: 10.1109/FRSE58934. 2023.00060.
[21] J. Xu and H. Wu, "Routing Resource Allocation for FPC in Complex Scenarios," 2023 4th International Conference on Electronic Communication and Artificial Intelligence (ICECAI), Guangzhou, China, 2023, pp. 46-51, doi: 10.1109/ICECAI58670.2023.10176480.
[22] K. -L. Wu, J. -S. Sun and G. -Y. Chen, "Flexible printed circuit board (FPC) antennas for mobile phone operation," 2010 5th International Microsystems Packaging Assembly and Circuits Technology Conference, Taipei, Taiwan, 2010, pp. 1-4, doi: 10.1109/IMPACT. 2010.5699636.
[23] Wenjie Sun, Fan Liu, Ziqi Ma, Chenghai Li, Jinxiong Zhou; Soft mobile robots driven by foldable dielectric elastomer actuators. J. Appl. Phys. 28 August 2016; 120 (8): 084901. https://doi.org/10.1063/1. 4960718
[24] Qu Y, Pan E, Zhu F, et al. Modeling thermoelectric effects in piezoelectric semiconductors: New fully coupled mechanisms for mechanically manipulated heat flux and refrigeration[J]. International journal of engineering science, 2023.
[25] Minaminosono T M S .Untethered rotational system with a stacked dielectric elastomer actuator[J].Smart Materials & Structures, 2021, 30(6).